that the natural level of expression of the CheZ gene is sufficient, without any further regulation, to dephosphorylate the right amount of CheY-P to adjust the system to the operational range of the motors.
27. P. Cluzel, M. Surette, S. Leibler, data not shown.
28. G. S. Waldo, B. M. Standish, J. Berendzen, T. C. Terwilliger, *Nature Biotechnol.* **17**, 691 (1999).
29. We thank U. Alon, N. Barkai, G. Bonnet, M. Elowitz, T. Griggs, C. Guet, T. Silhavy, J. Stock, J. Vilar, and E. Winfree for many helpful discussions and comments on the manuscript. This work was partially sponsored by the NIH. P.C. acknowledges support by a fellowship from the Program in Mathematics and Molecular Biology at the Florida State University, with funding from the NSF under grant DMS-9406348.

1 November 1999; accepted 14 January 2000

Salmonella Pathogenicity Island 2–Dependent Evasion of the Phagocyte NADPH Oxidase

Andrés Vazquez-Torres,[1] Yisheng Xu,[1] Jessica Jones-Carson,[1] David W. Holden,[2] Scott M. Lucia,[1] Mary C. Dinauer,[3] Pietro Mastroeni,[4]* Ferric C. Fang[1]†

A type III protein secretion system encoded by *Salmonella* pathogenicity island 2 (SPI2) has been found to be required for virulence and survival within macrophages. Here, SPI2 was shown to allow *Salmonella typhimurium* to avoid NADPH oxidase–dependent killing by macrophages. The ability of SPI2-mutant bacteria to survive in macrophages and to cause lethal infection in mice was restored by abrogation of the NADPH oxidase–dependent respiratory burst. Ultrastructural and immunofluorescence microscopy demonstrated efficient localization of the NADPH oxidase in the proximity of vacuoles containing SPI2-mutant but not wild-type bacteria, suggesting that SPI2 interferes with trafficking of oxidase-containing vesicles to the phagosome.

The central importance of the phagocyte NADPH (nicotinamide adenine dinucleotide phosphate) oxidase to innate host defense is vividly demonstrated in chronic granulomatous disease. Mutations in any of the subunits comprising the NADPH oxidase predispose patients to recurrent infections with fungi and bacteria, including *Salmonella* (*1*). The NADPH oxidase catalyzes the univalent reduction of oxygen to superoxide, an oxidizing species and precursor to potent antimicrobial molecules such as hydrogen peroxide, hydroxyl radical, and peroxynitrite (*2*, *3*). Pathogenic microbes have developed strategies to resist the antimicrobial effects of the NADPH oxidase, including the production of molecular scavengers, antioxidant enzymes, repair systems, and expression of specific antioxidant regulons (*2*). For example, the OxyR and SoxRS regulons enable *Escherichia coli* to resist the effects of hydrogen peroxide and superoxide, respectively (*4*). However, *S. typhimurium* does not require a functional OxyR or SoxRS regulon for virulence (*5*), suggesting that *Salmonella* may use alternative strategies to avoid exposure to high concentrations of phagocyte-derived oxidants in vivo.

A cluster of genes at centisome 30 of the *S. typhimurium* chromosome, designated *Salmonella* pathogenicity island 2 (SPI2), encodes a type III secretion system required for virulence and intracellular survival (*6*, *7*) and believed to translocate bacterial proteins into the cytosol of host cells. We have used immunodeficient mice to identify the specific host defenses targeted by products of the SPI2 genes. *Salmonella typhimurium* strains deficient at any of several SPI2 loci (*ssrA*, *ssaJ*, *ssaV*, *sseB*) (*8*) were found to be highly attenuated for virulence in C57BL/6 mice (Fig. 1A) (*9*). Virulence of these SPI2-mutant strains was not restored by administration of aminoguanidine, an inhibitor of inducible nitric oxide synthase (iNOS) (*10*), or by genetic abrogation of interferon-γ (IFN-γ) (*11*) or interleukin-12 (*12*) production (Fig. 1, B and C). In contrast, all four SPI2 mutants were able to cause lethal infection of congenic C57BL/6 mice deficient in the gp91*phox* subunit of the phagocyte NADPH oxidase (gp91*phox* knockout mice) (*13*) (Fig. 1D). Thus the SPI2 genes are not required for virulence in the absence of a phagocyte respiratory burst and might play a specific role in avoiding bacterial interaction with the NADPH oxidase.

Killing of isogenic *S. typhimurium* strains carrying mutations in various SPI2 genes (*ssaJ*, *sseA*, *sseB*, *ssrA*) was examined in macrophages from wild-type or respiratory burst-deficient mice (*14*). SPI2-mutant bacteria had increased susceptibility to killing by periodate-elicited murine peritoneal macrophages from C57BL/6 mice (Fig. 2A), but this enhanced

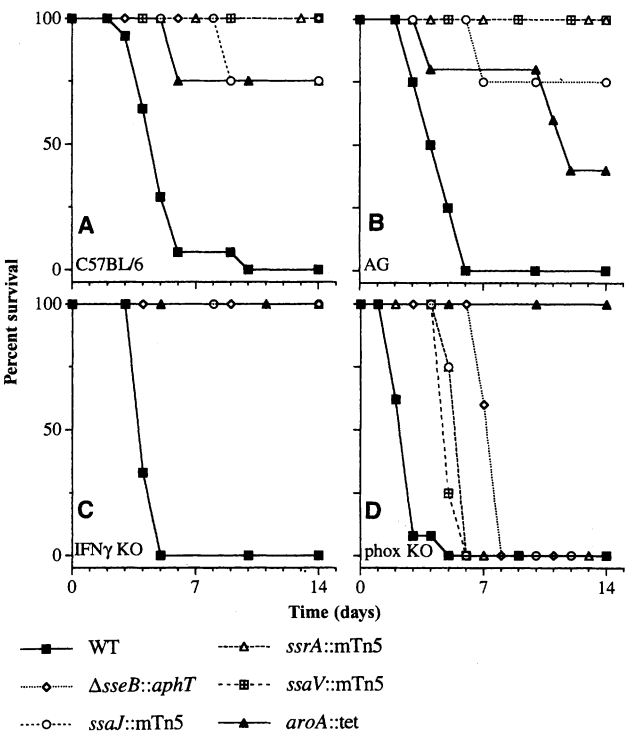

Fig. 1. Abrogation of the NADPH phagocyte oxidase restores virulence to SPI2-deficient *S. typhimurium* mutants. Survival curves are shown for wild-type C57BL/6 mice (**A**), wild-type mice fed drinking water containing the iNOS inhibitor aminoguanidine (**B**), congenic immunodeficient IFN-γ knockout mice (**C**) or gp91*phox* knockout mice (**D**), following intraperitoneal challenge with wild-type *S. typhimurium* or isogenic strains with mutations at *ssaJ*::Tn5, *ssaV*::Tn5, *ssrA*::Tn5, or Δ*sseB*::*aphT*. An isogenic *aroA*-mutant *S. typhimurium* strain with attenuated virulence in mice (*29*) was included as an additional control. These experiments used 4 to 14 mice per group.

[1]Departments of Medicine, Pathology, and Microbiology, University of Colorado Health Sciences Center, Denver, CO 80262, USA. [2]Department of Infectious Diseases, Imperial College School of Medicine, London W12 ONN, UK. [3]Indiana University School of Medicine, Indianapolis, IN 46202, USA. [4]Department of Biochemistry, Imperial College of Medicine and Technology, London SW7 2BZ, UK.

*Present address: Centre for Veterinary Science, University of Cambridge, Cambridge CB3 0ES, UK.
†To whom correspondence should be addressed. E-mail: ferric.fang@uchsc.edu

susceptibility was abrogated in macrophages from congenic gp91*phox* knockout mice (Fig. 2B). Parallel experiments using the NOS inhibitor N^G-monomethyl-L-arginine or macrophages from iNOS knockout mice did not restore wild-type levels of macrophage survival to the SPI2 mutants (*15*). Similar levels of NO-derived nitrite production were measured from macrophages infected with either wild-type or SPI2-mutant bacteria, indicating that SPI2 does not interfere with NO synthesis.

The SPI2 mutants were not more susceptible in vitro to hydrogen peroxide, the superoxide-generator methyl viologen, or the peroxynitrite-generator SIN-1 in disk diffusion assays and were not more susceptible to hydrogen peroxide killing in liquid medium (*16*). Thus SPI2 does not appear to directly enhance bacterial resistance to macrophage-derived oxidants. Furthermore, C57BL/6 peritoneal macrophages infected with a similar inoculum of wild-type or SPI2-mutant *Salmonella* exhibited comparable lucigenin-dependent chemiluminescence (*18*) (Fig. 3A). Infection with *Salmonella* was sufficient to stimulate a respiratory burst in periodate-elicited peritoneal macrophages. Superoxide production by macrophages infected with wild-type or *sseB*-mutant bacteria was approximately 0.013 and 0.009 nmol/hour per 10^5 macrophages, respectively, as measured by reduction of cytochrome c. Thus the SPI2 gene products might interfere with the localization rather than the activation of the phagocyte NADPH oxidase.

To visualize NADPH oxidase activity in relation to *Salmonella*-containing vacuoles, we performed ultrastructural studies of infected macrophages using cerium chloride (*19*). In the presence of hydrogen peroxide, cerium chloride is converted to electrodense cerium perhydroxide precipitate. Electron micrographs revealed efficient colocalization of cerium perhydroxide with vacuoles containing nonpathogenic *E. coli* W3110 (Fig. 3B) or SPI2-mutant *S. typhimurium* (Fig. 3, D and F), but not wild-type *S. typhimurium* (Fig. 3, C, E, and G). Approximately 50% of the vacuoles containing *sseB*-mutant *S. typhimurium* colocalized with cerium perhydroxide, contrasting with only 5% of those containing wild-type bacteria (Fig. 3H). The reduced tendency of vacuoles containing wild-type *Salmonella* to colocalize with cerium perhydroxide persisted despite augmented phagocyte stimulation with the potent NADPH oxidase activator phorbol 12-myristate 13-acetate (PMA) (Fig. 3, B, C, D, G, and H). Evidence of NADPH oxidase activity was seen in macrophages containing wild-type bacteria but was localized to empty vacuoles or to the plasma membrane (Fig. 3G). No cerium perhydroxide was detected in infected macrophages obtained from gp91*phox* knockout mice (*15*).

Intracellular distribution of the NADPH phagocyte oxidase following infection of macrophages with *Salmonella* was visualized by immunofluorescence microscopy (*20*). In quiescent cells, the NADPH oxidase p22 and p47 subunits appeared to be preferentially distributed in the plasma membrane and cytosol, respectively (Fig. 4, A and B), and were mobilized to the periphery upon activation with PMA (Fig. 4, C and D). In *Salmonella*-infected cells, the p22phox and p47phox subunits appeared to be localized within compartments that coalesced in the proximity of phagosomes containing green fluorescent protein (GFP)–expressing SPI2-mutant bacteria (Fig. 4, E and F). In contrast, the compartments containing the NADPH oxidase remained diffusely distributed within cells infected with GFP-expressing wild-type *Salmonella* (Fig. 4, G and H), or aggregated at intracellular locations remote from the bacteria (Fig. 4G). Localization of NADPH oxidase components was seen in the vicinity of 56% of *sseB*-mutant and 10% of wild-type bacteria, respectively, correlating well with the electron microscope studies. Thus, functional NADPH oxidase can be localized within discrete intracellular compartments in macrophages as has been described in human neutrophils (*21*). In-

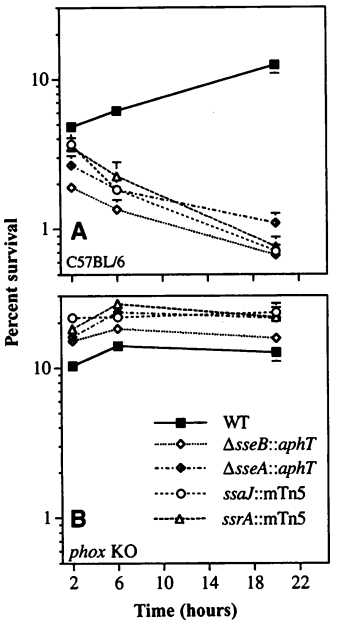

Fig. 2. Abrogation of the NADPH phagocyte oxidase restores the ability of SPI2-deficient *S. typhimurium* mutants to survive in macrophages. The survival of wild-type *S. typhimurium* 12023 or isogenic SPI2-deficient strains with mutations at *ssaJ*::Tn5, *ssrA*::Tn5, Δ*sseA*::*aphT*, and Δ*sseB*::*aphT* was measured in macrophages from C57BL/6 (**A**) and congenic gp91*phox* knockout mice (**B**). These data represent the mean ± SEM of three separate experiments.

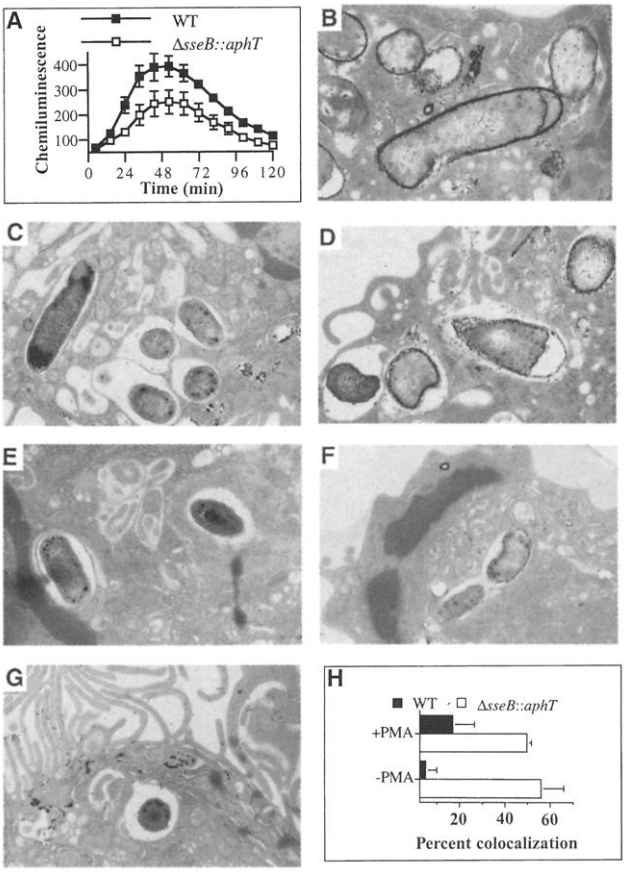

Fig. 3. Exclusion of oxyradical formation from *Salmonella*-containing vacuoles. Macrophages from C57BL/6 mice challenged with wild-type or *sseB*-mutant bacteria produced comparable quantities of superoxide as measured by reduction of lucigenin (arbitrary units for chemiluminescence) (**A**). NADPH oxidase activity was visualized as cerium perhydroxide precipitate in periodate-elicited macrophages from C57BL/6 mice challenged with either avirulent *E. coli* W3110 (**B**), wild-type *S. typhimurium* (**C**, **E**, and **G**), or isogenic *sseB*-mutant *S. typhimurium* (**D** and **F**). Cerium perhydroxide precipitate was localized to the plasma membrane (**G**) and to uninfected vacuoles in macrophages harboring wild-type *Salmonella*. In some experiments (**B** to **D** and **G**), the macrophages were activated *in vitro* with 20 ng/ml PMA (*30*). (B) and (D) are magnified ×10,752 (original magnification, ×49,250); (C), (E), (F), and (G) are magnified ×7968 (original magnification, ×36,500). The percentage of bacteria-containing vacuoles colocalizing with cerium perhydroxide precipitate as an indication of NADPH oxidase activity is shown in (**H**). These data represent 190 vacuoles from eight separate experiments.

traphagosomal oxyradical production appears to require both recruitment of cytosolic components to the membrane-associated flavocytochrome and intracellular vesicular trafficking to deliver active oxidase to the phagosome.

Other type III secretion systems have been shown to target the host cytoskeleton (*22*), and it is possible that SPI2 gene products originating from intraphagosomal bacteria (*23*) interfere with localization of the NADPH oxidase in phagocyte vacuolar membranes by blocking cytoskeletal rearrangements (*24*). The effects of this action are not necessarily limited to the NADPH oxidase and, indeed, could provide a common mechanism to explain observations suggesting that *S. typhimurium* interferes with the fusion of phagosomes with secondary lysosomes carrying markers such as the mannose-6-phosphate receptor and cathepsin (*25*). Such oxidase-independent effects of SPI2 might help to explain the slight delay in mortality caused by SPI2-mutant bacteria in gp91*phox* knockout mice (Fig. 1D), and the modest survival defect of SPI2 mutants in some cell lines lacking detectable production of reactive oxygen intermediates (*7*).

Overall, SPI2 appears to prevent the phagocyte NADPH oxidase from trafficking toward *Salmonella*-containing vacuoles, both reducing the oxidant stress encountered by *Salmonella* and potentially enhancing collateral oxidative damage to host tissues. Interference with the localization of the NADPH oxidase is coupled with more conventional antioxidant strategies such as scavengers, detoxifying enzymes, and repair systems (*2*, *26*). The ability of *Salmonella* to limit its exposure to high concentrations of toxic phagocyte-derived oxidants may help to explain the dispensability of catalase (*17*) and the SoxRS and OxyR oxidative stress regulons (*5*) for virulence. It is possible that other intracellular pathogens pursue similar strategies. For example, *Mycobacterium tuberculosis* is susceptible to reactive oxygen intermediates in vitro (*27*), but lacks a functional OxyR locus and appears to be relatively protected from effects of the NADPH oxidase in vivo (*28*). Exclusion of the NADPH oxidase from phagosomes may be an important contributor to the virulent nature of intracellular pathogens.

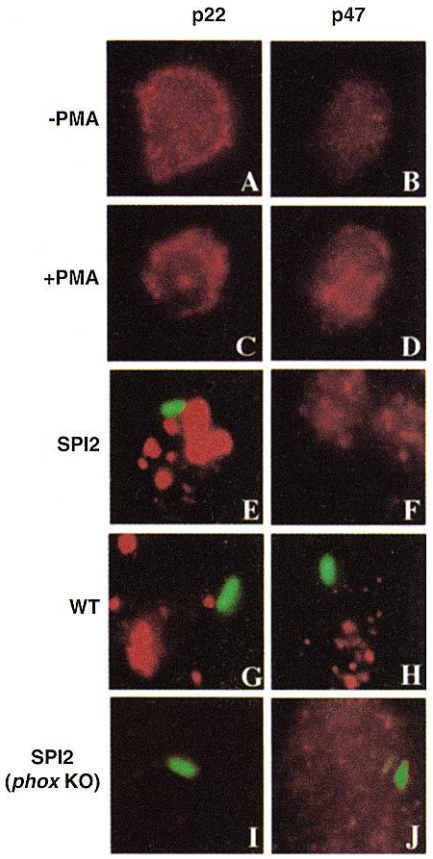

Fig. 4. Exclusion of the NADPH phagocyte oxidase from *Salmonella*-containing vacuoles. Immunofluorescence microscopy of p22 and p47 NADPH oxidase subunits (red) was performed in quiescent (**A** and **B**) and PMA-activated (**C** and **D**) macrophages. Both NADPH oxidase p22phox (**E**) and p47phox (**F**) subunits coalesced in the vicinity of GFP-positive (green) *sseB*-deficient *S. typhimurium*, contrasting with the dispersed pattern of vesicular distribution in the cytoplasm of macrophages infected with GFP-expressing (green) wild-type bacteria (**G** and **H**). (**I**) and (**J**) show p22phox and p47phox staining in macrophages from gp91*phox* knockout (*phox* KO) mice infected in vitro with *sseB*-mutant *S. typhimurium*. Magnification of fluorescence micrographs is ×1900 (original magnification, ×4000). These data are representative of 150 cells from 14 separate experiments.

References and Notes

1. R. Mouy, A. Fischer, E. Vilmer, R. Seger, C. Griscelli, *J Pediatr*. **114**, 555 (1989); J. T. Curnutte, P. J. Scott, B. M. Babior, *J. Clin. Invest*. **83**, 1236 (1989).
2. R. A. Miller and B. E. Britigan, *Clin. Microbiol. Rev*. **10**, 1 (1997).
3. H. Ischiropoulos, L. Zhu, J. S. Beckman, *Arch. Biochem. Biophys*. **298**, 446 (1992).
4. M. F. Christman, G. Storz, B. N. Ames, *Proc. Natl. Acad. Sci. U.S.A*. **86**, 3484 (1985); J. Wu and B. Weiss, *J. Bacteriol*. **173**, 2864 (1991).
5. S. I. Miller, A. M. Kukral, J. J. Mekalanos, *Proc. Natl. Acad. Sci. U.S.A*. **86**, 5054 (1989); F. C. Fang, A. Vazquez-Torres, Y. Xu, *Infect. Immun*. **65**, 5371 (1997); P. D. Taylor, C. J. Inchley, M. P. Gallagher, *Infect. Immun*. **66**, 3208 (1998).
6. M. Hensel *et al.*, *Science* **269**, 400 (1995); M. Hensel *et al.*, *Mol. Microbiol*. **30**, 163 (1998).
7. D. M. Cirillo, R. H. Valdivia, D. M. Monack, S. Falkow, *Mol. Microbiol*. **30**, 175 (1998); H. Ochman, F. C. Soncini, F. Solomon, E. A. Groisman, *Proc. Natl. Acad. Sci. U.S.A*. **93**, 7800 (1996).
8. SPI2-deficient *S. typhimurium* strains used in this study are derived from *S. typhimurium* 12023 (synonymous with ATCC 14028s). The construction of the SPI2 mutants is described in (*6*). The *ssrA* locus encodes a putative regulator of SPI2 gene expression, *ssaJ* and *ssaV* encode components of the secretory apparatus, and *sseB* encodes a secreted, surface-localized protein thought to be a translocon component [C. R. Beuzón *et al.*, *Mol. Microbiol*. **33**, 806 (1999)]. *Salmonella typhimurium* strain CL1509 deficient in *aroA* was originally constructed from wild-type *S. typhimurium* ATCC 14028s [R. M. Tsolis, A. J. Bäumler, I. Stojiljkovic, F. Heffron, *J. Bacteriol*. **177**, 4628 (1995)].
9. Viability of C57BL/6 mice, or congenic IFN-γ knockout mice, or gp91*phox* knockout mice that are susceptible to several attenuated *Salmonella* strains (*10*, *29*) was recorded daily after intraperitoneal challenge with 500 to 600 colony-forming units of wild-type or mutant *S. typhimurium*. The iNOS inhibitor aminoguanidine (Sigma-Aldrich, St. Louis, MO) (2.5% w/v) was added to the drinking water as indicated.
10. D. J. Wolff and A. Lubeskie, *Arch. Biochem. Biophys*. **316**, 290 (1995); M. A. DeGroote, T. Testerman, Y. Xu, G. Stauffer, F. C. Fang, *Science* **272**, 414 (1996).
11. D. K. Dalton *et al.*, *Science*, **259**, 1739 (1993).
12. P. Mastroeni, unpublished results.
13. J. D. Pollock *et al.*, *Nature Genet*. **9**, 202 (1995).
14. Killing of normal mouse serum–opsonized *S. typhimurium* by periodate-elicited peritoneal macrophages from C57BL/6, gp91*phox* knockout (*13*) and iNOS knockout [J. D. MacMicking *et al.*, *Cell* **81**, 641 (1995)] mice was estimated as described [M. A. DeGroote *et al.*, *Proc. Natl. Acad. Sci. U.S.A*. **94**, 13997 (1997)]. In selected experiments, 250 μM N^G-monomethyl-L-arginine was used to inhibit nitric oxide synthesis, which was confirmed by abrogation of nitrite production assayed with the Griess reagent.
15. A. Vazquez-Torres *et al.*, results not shown.
16. Disk diffusion susceptibility assays and killing by hydrogen peroxide in liquid medium were assayed as described [M. A. DeGroote *et al.*, *Proc. Natl. Acad. Sci. U.S.A*. **92**, 6399 (1995)] (*17*).
17. N. A. Buchmeier *et al.*, *J. Clin. Invest*. **95**, 1047 (1995).
18. Macrophage superoxide production was estimated by the reduction of 12.5 μM lucigenin (bis-*N*-methylacridinium) [Y. Li *et al.*, *J. Biol. Chem*. **273**, 2015 (1998)] (Sigma-Aldrich) with a Lumistar chemiluminometer (BMG Lab Technologies, Durham, NC) in Microlite flat-bottom microtiter plates (Dynex Technologies, Inc., Chantilly, VA) using wild-type or mutant *S. typhimurium* as stimuli. Macrophages from gp91*phox* knockout mice were used as negative controls (data not shown).
19. Ultrastructural studies [R. T. Briggs, D. B. Drath, M. L. Karnovsky, M. J. Karnovsky, *J. Cell Biol*. **67**, 566 (1975)] were performed in 24-well plates (Becton Dickinson Labware) with periodate-elicited macrophages (aged 48 hours) from C57BL/6 mice challenged for 1 hour with wild-type or Δ*sseB*-mutant *S. typhimurium*. The macrophages were washed with 0.1 M Tris maleate buffer, pH 7.5 at 37°C, preincubated with 0.1 M Tris maleate, 7% (w/v) sucrose, 1 mM aminotriazole buffer, pH 7.5, for 10 min at 37°C, and subsequently incubated with 0.1 M Tris maleate, 7% (w/v) sucrose, 1 mM aminotriazole, 1 mM $CeCl_3$, 0.71 mM NADH, 0.71 mM NADPH buffer, pH 7.5, for 20 min at 37°C, followed by a wash with 0.1 M Tris maleate, 7% sucrose (all reagents from Sigma-Aldrich). The cells were fixed in 2% glutaraldehyde in phosphate-buffered saline (PBS), postfixed in 1% OsO_4 in PBS, dehydrated in graded ethanols, and embedded in a Spurr's low viscosity epoxy resin. Counterstaining was performed with uranyl acetate and lead citrate. Ultrathin sections were cut with an LKB ultramicrotome III and examined in a Philips EM201 electron microscope.
20. Wild-type or *sseB*-mutant *S. typhimurium* expressing GFP were used for fluorescence studies. Macrophages placed onto cover slips were infected with GFP-expressing *S. typhimurium* strains as above. The cells were fixed after 90 min of infection with 2% paraformaldehyde in PBS, washed with 0.1% Tween in PBS, incubated with a 3% normal goat serum solution, and stained with 5 μg/ml of a rabbit anti-p22phox or p47phox polyclonal antibody (gift of P. Heyworth), followed by a rhodamine-conjugated goat anti-rabbit polyclonal antibody (Jackson Immunoresearch Laboratories, West Grove, PA). After washing, the cover slips were mounted with Vectashield (Vector Laboratories, Burlingame, CA) and examined with an Olympus IX70 inverted microscope, a Photometrics PXL camera with Kodak KAF1400 chip, and a Silicon Graphic O_2 computer with DeltaVision deconvolution software (Applied Precision, Seattle, Washington).
21. A. J. Jesaitis *et al.*, *J. Clin. Invest*. **85**, 821 (1990); T. Kobayashi, J. M. Robinson, H. Seguchi, *J. Cell Sci*. **111**, 81 (1998); C. Vaissiere, V. Le Cabec, I. Marionneau-Parini, *J. Leukocyte Biol*. **65**, 629 (1999).
22. J. E. Galán and R. Curtiss III, *Proc. Natl. Acad. Sci. U.S.A*. **86**, 6383 (1989); D. Zhou, M. S. Mooseker, J. E. Galán, *Science* **283**, 2092 (1999).
23. R. H. Valdivia and S. Falkow, *Science* **277**, 2007 (1997).
24. M. E. Wiles, J. A. Dykens, C. D. Wright, *Life Sci*. **57**,

1533 (1995); S. Dusi, V. Della Bianca, M. Donini, K. A. Nadalini, F. Rossi, *J. Immunol.* **157**, 4615 (1996); L. A. H. Allen *et al.*, *Blood* **93**, 3521 (1999).
25. N. A. Buchmeier and F. Heffron, *Infect. Immun.* **59**, 2232 (1991); F. Garcia-del Portillo and B. B. Finlay, *J. Cell Biol.* **129**, 81 (1995); K. Uchiya *et al. EMBO J.* **18**, 3924 (1999).
26. F. C. Fang, *J. Clin. Invest.* **99**, 2818 (1997).
27. T. R. Garbe, N. S. Hibler, V. Deretic, *Mol. Med.* **2**, 134 (1996).
28. S. O'Brien, P. S. Jackett, D. B. Lowrie, P. W. Andrew, *Microb. Pathog.* **10**, 199 (1991).
29. S. K. Hoiseth and B. A. Stocker, *Nature* **291**, 238 (1981); J. L. VanCott *et al. Nature Med.* **4**, 1247 (1998).
30. J. A. Cox, A. Y. Jeng, N. A. Sharkey, P. M. Blumberg, A. I. Tauber *J. Clin. Invest.* **76**, 1932 (1985).
31. We thank A. Jones, W. Betz, and S. Fadul for assistance with microscopy, B. Hybertson for the use of a chemiluminometer, F. Heffron for the gift of strain CL1509, L. A. Allen for helpful discussions, and R. Faust and P. Heyworth for the antibody against p47phox. This work was supported by an NIH postdoctoral fellowship, NIH grants AI39557 and AI44486, the James Biundo Foundation, and grants from Biotechnology and Biological Sciences Research Council, the Wellcome Trust, and the Medical Research Council (UK).

8 November 1999; accepted 18 January 2000

Resonant Formation of DNA Strand Breaks by Low-Energy (3 to 20 eV) Electrons

Badia Boudaïffa, Pierre Cloutier, Darel Hunting, Michael A. Huels,* Léon Sanche

Most of the energy deposited in cells by ionizing radiation is channeled into the production of abundant free secondary electrons with ballistic energies between 1 and 20 electron volts. Here it is shown that reactions of such electrons, even at energies well below ionization thresholds, induce substantial yields of single- and double-strand breaks in DNA, which are caused by rapid decays of transient molecular resonances localized on the DNA's basic components. This finding presents a fundamental challenge to the traditional notion that genotoxic damage by secondary electrons can only occur at energies above the onset of ionization, or upon solvation when they become a slowly reacting chemical species.

The genotoxic effects of ionizing radiations (β-, x-, or γ-rays) in living cells are not produced by the mere direct impact of the primary high-energy quanta. Instead, mutagenic, recombinogenic, and other potentially lethal DNA lesions (*1–3*), such as single- and double-strand breaks (SSBs and DSBs), are induced by secondary species generated by the primary ionizing radiation (*4*). Free secondary electrons, with energies between ~1 and 20 eV, are the most abundant (~5×10^4 per MeV) of these secondary species (*5–8*), but it is unclear whether such low-energy electrons are able to induce genotoxic damage, such as SSBs or DSBs (*9*). To investigate this question, we have irradiated plasmid DNA with a very low energy electron (LEE) source under ultrahigh vacuum (UHV) conditions, because condensed-phase electron-molecule interactions are highly sensitive to minor impurities (*10*, *11*). Our previous work on small bio-organic molecules (*12–15*) allowed us to develop and adapt the necessary electron microbeam techniques to determine the effects of very low energy, nonthermal secondary electrons on the entire DNA molecule at various well-defined incident electron energies between 3 and 20 eV. The experiments were performed at 10^{-9} torr in a hydrocarbon-free environment, and all sample manipulation occurred in a sealed glove box under a pure dry nitrogen atmosphere.

Plasmid DNA [pGEM 3Zf(−), 3199 base pairs] was extracted from *Escherichia coli* DH5α, purified, and resuspended in nanopure water (without any tris or EDTA). An aliquot of this pure aqueous DNA solution was deposited onto chemically clean tantalum substrates held at liquid nitrogen temperatures, lyophilized with a hydrocarbon-free sorption pump at 0.005 torr (*16*), and transferred directly to the UHV chamber without exposure to air or further characterization. After evacuation (~24 hours), the room-temperature DNA solids were irradiated with a monochromatic LEE beam for a specific time at a fixed beam current density (2.2×10^{12} electrons s^{-1} cm^{-2}) and incident electron energy. Thus, the LEE irradiations were performed on clean DNA containing its structural water (*17*). The DNA was then analyzed by agarose gel electrophoresis and quantified as supercoiled (undamaged), nicked circle (SSB), full-length linear (DSB), and short linear forms; the first three species produce well-resolved bands, whereas the latter produces a smear.

The measured DNA damage yields (Fig. 1) show three striking characteristics. First, very low energy electron irradiation can induce substantial damage in DNA, namely SSBs and DSBs, even at electron energies well below the ionization limit of DNA (7.5 to 10 eV) (*18*). Second, DNA damage by 3- to 20-eV electrons is highly dependent on the initial kinetic energy of the incident electron, particularly below 14 to 15 eV, where we observed thresholds near 3 to 5 eV and intense peaks near 10 eV. This is in sharp contrast to DNA strand breaks induced by similarly energetic photons, where both SSBs and DSBs have been found to increase monotonically above a threshold near 7 eV and remain relatively constant above ~12 eV (*19*), up to ~2 keV (*20*). Third, the SSB and DSB peak yield values measured here above 7 eV (8.2×10^{-4} and 2×10^{-4} strand breaks per incident electron, respectively, at the 10-eV peak) are roughly one to two orders of magnitude larger than those for 10- to 25-eV photons (*20*). For 7- to 25-eV photons, the ratio of SSBs to DSBs is about 30:1, whereas for 7- to 20-eV electrons it is about 4:1 on average. Thus, the mechanisms of DNA damage depend not only on the quantum of energy absorbed, but also on the nature of the particle that deposits the energy.

The strong electron energy dependence of the DNA strand breaks, observed here below 14 eV, is attributed to electron attachment somewhere within the DNA molecule, followed by localized bond rupture and subsequent reactions of the fragmentation products. Electron attachment (*21*) is best illustrated by the type of damage it induces in thin films consisting of very small molecules, such as thymine (*13*), H_2O (*22*), or a deoxyribose analog (*14*) (Fig. 2). These and other electron impact experiments (*15*), including some on small linear (*23*, *24*) and cyclic (*11*, *12*, *25*) hydrocarbons, have shown that electrons with energies below 15 eV initiate fragmentation of small molecules essentially by attachment of the incident electron; this leads to the formation of a resonance, namely, a transient molecular anion (TMA) state. For a molecule RH this corresponds to $e^- + RH \rightarrow RH^{*-}$, where the RH^{*-} has a repulsive potential along the R-H bond coordinate. This TMA can decay by electron autodetachment (*26*) or by dissociation along one, or several (*12*, *14*, *25*), specific bonds such as $RH^{*-} \rightarrow R^{\cdot} + H^-$.

The probability for attachment and subsequent decay via either channel is in part defined by the repulsiveness of the RH^{*-} potential energy surface and its uncertainty energy width $\Gamma = \hbar/\tau$, where $\hbar$ is Planck's constant divided by 2π and τ is the electron autodetachment

Canadian Medical Research Council Group in Radiation Sciences, Department of Nuclear Medicine and Radiobiology, Faculty of Medicine, University of Sherbrooke, Québec J1H 5N4, Canada.

*To whom correspondence should be addressed. E-mail: mhuels01@courrier.usherb.ca